Coronary artery segmentation and stenosis quantification in CT images with use of a right generalized cylinder model

Leonardo Flórez-Valencia[1], Maciej Orkisz[2], Ricardo A. Corredor Jerez[2,3], Juan S. Torres González[3], Esteban M. Correa Agudelo[3], Claire Mouton[2], and Marcela Hernández Hoyos[3]

[1] Grupo Takina, Dept° Sistemas, Pontificia Universidad Javeriana, Bogotá, Colombia
[2] Université de Lyon, CREATIS; CNRS UMR 5220; INSERM U 1044; INSA-Lyon; Université Lyon 1, France
[3] Grupo Imagine, Grupo GIB, Universidad de los Andes, Bogotá, Colombia

Abstract. The proposed method is semi-automatic, as it requires the artery endpoints as input. Its outline is as follows. First, a centerline is extracted between the endpoints, using a modified minimal path approach. Second, 2D contours are extracted in planes orthogonal to the centerline, using a Fast-Marching algorithm with an appropriately tailored speed function and stopping criterion. Third, the contours are used to reconstruct a regularized continuous 3D surface based on a Right Generalized Cylinder model. The contour extraction and the regularization of the model parameters are driven by a Kalman filter. Next, an "idealized" cylinder is reconstructed based on a linear regression of the radii of the most reliable contours. Finally, the stenoses are detected and quantified by comparing the actual and idealized cylinder. The method was evaluated on 24 datasets from the Coronary Artery Algorithm Evaluation Framework. It achieved a moderate segmentation accuracy (Dice similarity index 51%), but a poor stenosis detection rate (sensitivity 34%).

Keywords: minimum cost paths, front propagation, Kalman estimator

1 Introduction

The computed tomography angiography (CTA) images are increasingly used to diagnose the coronary artery disease. Nevertheless, the detection and assessment of the coronary stenoses is time consuming and prone to errors. Various (semi-) automatic image processing techniques can assist the physicians in the detection and quantification of the lesions. Extraction of the artery centerline is a key to "unroll" the artery and generate a so-called curved planar reformation (CPR) display, which is very helpful to visually assess the arteries. The centerline is also frequently used as input to subsequent segmentation and/or detection stages. The "3D Segmentation in the Clinic Grand Challenge II" held at the 11th MICCAI conference in September 2008 [8] demonstrated a good performance of the best existing centerline extraction methods. Among these methods, a frequently

adopted approach associates a minimum-cost path search and the use of a medialness criterion derived from the gradient flux computation. This was confirmed by a survey published the same year [7]. Attempts to accurately delineate the coronary artery lumen and to detect the stenoses in CTA images have been less frequent and less successful. Often, strong assumptions have been made on the cross-sectional shape and/or appearance. Some authors preferred a direct detection of anomalous sections without actual segmentation, regardless the nature of lesions (calcified or hypodense) and the stenosis degree [10].

Our method is semi-automatic, as it requires the artery endpoints as input. Its outline is as follows. First, a centerline is extracted between the endpoints, using a modified minimal path approach. Second, 2D contours are extracted in planes orthogonal to the centerline, using a Fast-Marching algorithm with an appropriately tailored speed function and stopping criterion. Third, the contours are used to reconstruct a regularized continuous 3D surface based on a Right Generalized Cylinder state model (RGC-sm) [1]. Both the contour extraction and the regularization of the model parameters are driven by a Kalman filter. Next, an "idealized" cylinder is reconstructed based on a linear regression of the radii of the most reliable contours. The stenoses are then detected and quantified by comparing the actual and idealized cylinder. Finally, the model is triangulated to generate the final mesh representation.

2 Initial axis extraction

The minimum-cost path approach is usually associated with a front-propagation strategy, which can be performed by a *Fast-Marching* (FM) algorithm, followed by a backtracking from the endpoint to the starting point across the arrival time map [3]. Equivalently, *Dijkstra's* algorithm can be used to compute a minimum spanning tree from a graph built of the image voxels as nodes, with an associated cost function [4]. The propagation speed has to be high (the cost has to be low) along the arteries and low in the cross-sectional directions. The choice of an appropriate speed function is a key problem in this approach.

We actually use the Dijkstra's algorithm to find the minimal paths. To define the cost function $\mathcal{F}(\mathbf{p})$ in each voxel $\mathbf{p}$, we use the medialness function $m(\mathbf{p})$ proposed in [5], where the image gradient norm is analyzed along concentric rays in order to find the best radius that models the vessel as a cylinder. As this function produces high values in voxels near the center of the vessel, it is converted to a cost function as follows: $\mathcal{F}(\mathbf{p}) = \alpha \exp\left(-\frac{m(\mathbf{p})}{\beta}\right)$, where α and β are used to control the function selectivity. To guarantee the smoothness of the final path, a Bézier curve $\mathcal{B}$ is used.

3 Cross-sectional contour extraction

The planar contours are extracted using the FM front propagation technique [9], which needs the definition of a potential field $\mathcal{P}(\mathbf{p})$ expected to be maximum at

discontinuities (edges) and minimum within uniform regions. We use:

$$\mathcal{P}(\mathbf{p}) = \gamma \exp\left(-\frac{|\nabla f(\mathbf{p})|\, sign((\mathbf{p}-\hat{\mathbf{h}})\cdot\nabla f(\mathbf{p}))}{\delta}\right), \tag{1}$$

which is designed to push the contour towards pixels with large gray-level gradients $\nabla f(\mathbf{p})$, while keeping them from "climbing" or "descent" zones, with contrasts that do not represent vessels. Such contrasts are defined by the parameters γ and δ. FM is performed in the plane passing through the predicted point $\hat{\mathbf{h}} \in \mathcal{B}$, and oriented according to the Frenet frame $\mathbf{Fr}$ associated to $\mathcal{B}$. The FM propagation should be stopped at time value T when the growth of the area A encompassed by the front becomes very slow, which is characterized by a large value of $\Delta T/\Delta A$. Actually, at each iteration we compute the mean $\mu_{T/A}$ and the standard deviation $\sigma_{T/A}$ of $\Delta T/\Delta A$ and the propagation stops when $\Delta T/\Delta A > \mu_{T/A} + 10\sigma_{T/A}$ [2]. Summarizing, a *discrete* contour $\mathcal{C}$ defined as a set of *ordered* points is extracted as follows:

1. The potential field $\mathcal{P}(\mathbf{p})$ is calculated in 3D and cut by the plane passing by $\hat{\mathbf{h}}$ and oriented by the first column vector of $\mathbf{Fr}$, to obtain a 2D image $\mathcal{Q}(\mathbf{p})$.
2. The FM algorithm is executed on $\mathcal{Q}(\mathbf{p})$ with $\hat{\mathbf{h}}$ as the first trial point (front initialization).
3. The FM generates a level set $\mathcal{L}(\mathbf{p})$ which contains $\mathcal{C}$ as its last level.

4 Right generalized cylinder model

The RGC-sm model is an association of a generating curve $\mathcal{H}$ and a stack of contours describing the surface $\mathcal{S}$. The model is piecewise, *i.e.* it assumes that a generalized cylinder can be subdivided into pieces such that the model parameters be constant within each piece separately. Each piece $\mathcal{H}_i$ of the generating curve is thus a helix defined by its length Δ_i, curvature κ_i, torsion τ_i and by the azimuthal rotation angle ν_i of the local basis $\boldsymbol{\Gamma}_i(t)$ attached to $\mathcal{H}_i$, with respect to the corresponding Frenet frame. Each piece $\mathcal{S}_i$ of the surface is a continuous stack of contours $\mathbf{c}_i(t,\omega)$ defined by a tuple $\{\mathbf{Z}_i, \boldsymbol{\Lambda}_i\}$, where $\mathbf{Z}_i = \{z_{i,l} \in \mathbb{C}; -q \le l \le +q\}$ represents the Fourier coefficients describing the first contour in the piece, and $\boldsymbol{\Lambda}_i = \{\lambda_{i,l} \in \mathbb{C}; -q \le l \le +q\}$ is an ordered set of $2q+1$ coefficients linearly transforming the contour along $\mathcal{H}_i$:

$$\mathbf{c}_i(t,\omega) = \sum_{l=-q}^{+q} (\lambda_{i,l}(t-t_i) + z_{i,l}) e^{jl\omega}, \tag{2}$$

where t and ω respectively are arc-length and azimuthal parameters. The number q of harmonics controls the level of details of the contours, and thus of the whole generalized cylinder surface. Each surface piece $\mathcal{S}_i$ is connected to the corresponding generating curve piece $\mathcal{H}_i$ by the following equation:

$$\mathbf{s}_i(t,\omega) = \boldsymbol{\Gamma}_i(t) \cdot \begin{bmatrix} 0 \\ \mathtt{Re}(\mathbf{c}_i(t,\omega)) \\ \mathtt{Im}(\mathbf{c}_i(t,\omega)) \end{bmatrix} + \mathbf{h}_i(t), \tag{3}$$

where $\mathbf{h}_i(t)$ is the spatial location of the origin of $\boldsymbol{\Gamma}_i(t)$, which belongs to $\mathcal{H}_i$. The entire model is thus:

$$\mathcal{M} \equiv \{\mathbf{h}_0, \boldsymbol{\Gamma}_0, \mathbf{Z}_0, \{\kappa_i, \tau_i, \nu_i, \Delta_i, \boldsymbol{\Lambda}_i;\ 0 \leq i < n\}\}, \tag{4}$$

where $\mathbf{h}_0 \equiv \mathbf{h}_0(t=0)$ is the first point of $\mathcal{H}$, $\boldsymbol{\Gamma}_0 \equiv \boldsymbol{\Gamma}_0(t=0)$ is the first basis attached to $\mathbf{h}_0$ and $\mathbf{Z}_0 \equiv \mathbf{Z}_0(t=0)$ is the Fourier decomposition of the first RGC contour.

The initialization of the RGC-sm reconstruction process requires $\mathbf{h}_0$, $\boldsymbol{\Gamma}_0$ and $\mathbf{Z}_0$. One of the seed-points (typically the proximal one) is taken as $\mathbf{h}_0$. The orthonormal basis $\boldsymbol{\Gamma}_0$ is constructed such that its first vector is tangent to $\mathcal{B}$ in $\mathbf{h}_0$, the second vector is oriented along $\mathbf{h}_0 - \mathbf{c}_{0,0}$, where $\mathbf{c}_{0,0}$ is the first point of the contour $\mathcal{C}_0$, and the third vector is orthogonal to both. $\mathbf{Z}_0$ is calculated as the Fourier series corresponding to $\mathcal{C}_0$, using the harmonics up to the third order ($q = 3$), which is sufficient to represent reasonably complex cross-sections.

5 Calculation of model parameters

Without loss of generality, we describe the process for the cylinder piece defined by the first pair of contours. We first compute the transition operators, respectively rotation and translation, between the extremities:

$$\boldsymbol{\Phi}(0, \Delta_0) = \boldsymbol{\Gamma}_0^\top \cdot \boldsymbol{\Gamma}_1, \tag{5}$$

$$\mathbf{Tr}(0, \Delta_0) = \boldsymbol{\Gamma}_0^\top \cdot (\mathbf{h}_1 - \mathbf{h}_0). \tag{6}$$

$\boldsymbol{\Phi}$ is a rotation operator and one of the properties of the rotation matrices is the existence of Θ and $\boldsymbol{\Xi}$ such that $\boldsymbol{\Phi}(0,\Delta_0) - \boldsymbol{\Phi}(0,\Delta_0)^\top = 2\sin\Theta \cdot \boldsymbol{\Xi}$, where Θ is the rotation angle and the non-zero elements of the antisymmetric matrix $\boldsymbol{\Xi}$ compose the vector defining the rotation axis. Moreover, it can be demonstrated that $\boldsymbol{\Phi}(t_1, t_2) = \exp((t_2 - t_1) \cdot \boldsymbol{\Psi})$, where $\boldsymbol{\Psi}$ is proportional to $\boldsymbol{\Xi}$: $\boldsymbol{\Psi} = \zeta\boldsymbol{\Xi}$. In the case where $\boldsymbol{\Phi}$ describes the rotation between two frames attached to a helix, the curvature and torsion of the helix are proportional (via ζ) to the cosine and sine of the angle φ that represents the "slope" of the helix. Hence, the second step is the subtraction:

$$\boldsymbol{\Phi}(0,\Delta_0) - \boldsymbol{\Phi}(0,\Delta_0)^\top = \begin{bmatrix} 0 & -c & b \\ c & 0 & -a \\ -b & a & 0 \end{bmatrix} \Rightarrow \Theta = \arcsin\left(\sqrt{a^2+b^2+c^2}/2\right).$$

It can be demonstrated that a, b, c can be used to calculate φ, then ζ:

$$\varphi = \arcsin\left(a/\sqrt{a^2+b^2+c^2}\right), \qquad \zeta = \frac{\sin\Theta\cos^2\varphi + \Theta\sin^2\varphi}{\left[\boldsymbol{\Phi}(0,\Delta_0)\,[1\ 0\ 0]^\top\right]^\top \mathbf{Tr}(0,\Delta_0)},$$

which in turn permits us the computation of the axial parameters:

$$\begin{cases} \nu_0 &= \arctan(b/c), \\ \kappa_0 &= \zeta\cos\varphi, \\ \tau_0 &= \zeta\sin\varphi, \\ \Delta_0 &= \Theta/\zeta. \end{cases} \tag{7}$$

Numerical stability problems might arise when $\boldsymbol{\Phi}(0, \Delta_0) = \mathbf{I}$, which occurs when $\mathcal{H}_0$ is a straight line segment. This is checked after the computation of $\boldsymbol{\Gamma}_0$ and $\boldsymbol{\Gamma}_1$, and the parameters, in this case, are set as follows: $\left[\kappa_0 \; \tau_0 \; \nu_0 \; \Delta_0\right]^\top = \left[0 \; 0 \; 0 \; |\mathbf{h}_1 - \mathbf{h}_0|\right]^\top$. The last step is the computation of the parameters describing the linear evolution of the Fourier decomposition of the contours:

$$\boldsymbol{\Lambda_0} = \left\{ \frac{z_{1,l} - z_{0,l}}{\Delta} \in \mathbb{C} : -q \leq l \leq +q \right\}. \tag{8}$$

6 Kalman filtering

The *Kalman state estimator* (KSE) [6] is used to control the vessel tracking along an initial axis $\mathcal{B}$ extracted between the endpoints. It predicts the 3D locations, orientations and shapes of the contours that delimit the consecutive cylinder pieces. The observation vector, coding the RGC-sm parameters of the i-th piece, is computed from the result of the contour extraction performed in the predicted plane. The observation is then filtered by the KSE to produce a corrected estimate of the parameters, which is expected to smooth out the possible errors of the contours and initial axis extraction. Only the very first contour remains uncorrected.

The KSE adapts the tracking speed to the complexity of the local vascular shapes (axial and superficial). In complex shapes (high local changes of curvature, for example) the length of the cylinder piece is automatically reduced. This occurs when the predicted contours are too different from the observations.

7 Stenosis grading

During the Kalman filtering, an ideal vessel model is computed in order to compare it with the final constructed model.

The idea is as follows: along the Kalman filtering process, we can measure a confidence value that expresses how much the "a posteriori" state was corrected. If the confidence is high, we keep this contour (particularly, its area) together with its distance to the ostium. Then, a linear regression is performed in order to model the area change of perpendicular conturs along the vessel's central axis. The slope and intercept found in this step are used to construct a RGC model of circles with contours where the area has this linear behavior.

Then, the diameters of the final constructed model are compared to the diameters of this ideal cylinder. If the stenosis degree is in the range $[20, 100]$, the axis point and the stenosis degree are kept for clinical analysis.

8 Results

Stenosis detection and quantification, as well as lumen segmentation were evaluated on 24 testing datasets, available within the Coronary Artery Algorithm Evaluation Framework (http://coronary.bigr.nl). Figure 1 displays an example of segmentation result. Quantitative results are presented in tables 1, 2 and 3.

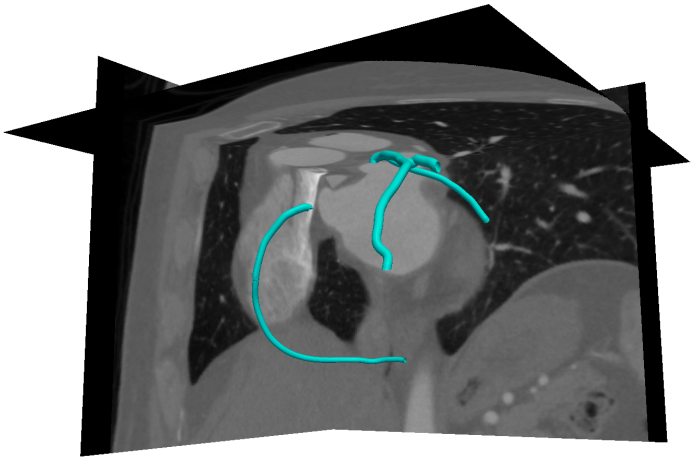

Fig. 1. Example of segmentation result.

Table 1. Stenosis detection results for dataset labeled as "testing1"

Calc. cat.	**QCA Sens.**		**QCA P.P.V.**		**CTA Sens.**		**CTA P.P.V.**		**Avg. rank**
	%	**rank**	**%**	**rank**	**%**	**rank**	**%**	**rank**	
0	0.00	1.0	0.00	1.0	0.00	1.0	0.00	1.0	1.0
1	0.00	1.0	0.00	1.0	0.00	1.0	0.00	1.0	1.0
2	0.50	1.0	0.14	1.0	0.00	1.0	0.00	1.0	1.0
3	0.44	1.0	0.12	1.0	0.00	1.0	0.00	1.0	1.0
4	1.00	1.0	0.30	1.0	0.00	1.0	0.00	1.0	1.0
All	**0.34**	**1.0**	**0.10**	**1.0**	**0.00**	**1.0**	**0.00**	**1.0**	**1.0**

9 Conclusions

RGC-sm is a powerful tool capable of concisely describing complex generalized cylindrical shapes. The theoretical framework permits the reconstruction of a continuous surface corresponding to the lumen, based on a stack of discrete contours. Additionally, the Kalman estimator permits a correction of the observation errors when these remain within a reasonable range. However, our current implementation of the image processing steps devised to provide the observations is clearly not optimal. Several errors are introduced by our segmentation method. In fact, the use of an always inflating deformable contour, such as the Fast Marching front, is uneasy, since the speed function and stopping criteria hardly can cope with all possible configurations (nearby veins, cavities, calcifications, etc.). Furthermore, 2D Fast Marching does not exploit the 3D continuity of the vascular lumen, which might be helpful in some complicated situations.

Table 2. Stenosis quantification results for dataset labeled as "testing1"

Calc. cat.	QCA Avg. Abs. diff.		QCA R.M.S. diff.		CTA Weighted Kappa		Avg. rank
	%	rank	%	rank	%	rank	
0	43.2	1.0	47.7	1.0	-0.01	1.0	1.0
1	46.4	1.0	47.9	1.0	-0.01	1.0	1.0
2	45.9	1.0	51.4	1.0	-0.02	1.0	1.0
3	43.9	1.0	48.3	1.0	-0.04	1.0	1.0
4	44.1	1.0	48.2	1.0	-0.05	1.0	1.0
All	**44.6**	**1.0**	**48.9**	**1.0**	**-0.02**	**1.0**	**1.0**

Acknowledgements

This work has been partly funded by ECOS Nord C11S01, Uniandes Interfacultades 06-2010 and Colciencias 1204-519-28996 grants and by the internal project PS3473 "Vitral IV" at the Pontificia Universidad Javeriana.

References

1. J. Azencot and M. Orkisz. Deterministic and stochastic state model of right generalized cylinder (RGC-sm): application in computer phantoms synthesis. *Graph. Models*, 65(6):323–350, 2003.
2. M. Baltaxe Milwer, L. Flórez-Valencia, M. Hernández Hoyos, I.E. Magnin, and M. Orkisz. Fast marching contours for the segmentation of vessel lumen in CTA cross-sections. In *Proc. Conf. IEEE Eng. Med. Biol. Soc.*, pages 791–794, Lyon, France, 2007. IEEE.
3. L.D. Cohen and R. Kimmel. Global minimum for active contour models: a minimal path approach. *Int J Comput Vision*, 24:57–78, 1997.
4. E.W. Dijkstra. A note on two problems in connexion with graphs. *Numerische Mathematik*, 1:269–271, 1959.
5. M.A. Gülsün and H. Tek. Robust vessel tree modeling. In *Proc. 11th Int. Conf. Med. Image Comput. Computer-Assisted Intervention - MICCAI*, volume LNCS 5241, pages 602–611, Berlin, Heidelberg, 2008. Springer-Verlag.
6. R.E. Kalman. A New Approach to Linear Filtering and Prediction Problems. *Trans ASME–J. Basic Engineering*, 82(Series D):35–45, 1960.
7. D. Lesage, E.D. Angelini, I. Bloch, and G. Funka-Lea. A review of 3D vessel lumen segmentation techniques: Models, features and extraction schemes. *Medical Image Analysis*, 13(1):819–845, 2009.
8. M. Schaap, C.T. Metz, T. van Walsum, A.G. van der Giessen, A.C. Weustink, N.R. Mollet, C. Bauer, H. Bogunović, C. Castro, X. Deng, E. Dikici, T. O'Donnell, M. Frenay, O. Friman, M. Hernández Hoyos, P.H. Kitslaar, K. Krissian, C. Kühnel, M.A. Luengo-Oroz, M. Orkisz, Ö. Smedby, M. Styner, A. Szymczak, H. Tek, C. Wang, S.K. Warfield, Y. Zhang, S. Zambal, G.P. Krestin, and W.J. Niessen. Standardized evaluation methodology and reference database for evaluating coronary artery centerline extraction algorithms. *Med Image Anal*, 13(5):701–714, 2009.
9. J.A. Sethian. A fast marching level set method for monotonically advancing fronts. In *Proc. Nat. Acad. Sci.*, volume 93, pages 1591–1595, 1996.

Table 3. Carotid arteries segmentation results for dataset labeled as "testing1"

Patient	DICE diseased		DICE healthy		MSD diseased		MSD healthy		MAXSD diseased		MAXSD healthy		Avg. rank
	%	rank	%	rank	%	rank	%	rank	%	rank	%	rank	
18	–	–	0.30	1.0	–	–	0.80	1.0	–	–	9.45	1.0	1.0
19	0.61	1.0	0.32	1.0	0.20	1.0	0.71	1.0	3.68	1.0	11.08	1.0	1.0
20	–	–	0.63	1.0	–	–	0.49	1.0	–	–	3.34	1.0	1.0
21	0.79	1.0	0.39	1.0	0.05	1.0	1.03	1.0	2.17	1.0	10.74	1.0	1.0
22	–	–	0.78	1.0	–	–	0.28	1.0	–	–	4.44	1.0	1.0
23	0.49	1.0	0.28	1.0	0.21	1.0	1.36	1.0	1.92	1.0	10.57	1.0	1.0
24	0.57	1.0	0.82	1.0	0.15	1.0	0.19	1.0	5.65	1.0	1.99	1.0	1.0
25	–	–	0.69	1.0	–	–	0.36	1.0	–	–	4.83	1.0	1.0
26	0.39	1.0	0.41	1.0	0.65	1.0	0.36	1.0	3.05	1.0	6.29	1.0	1.0
27	–	–	0.57	1.0	–	–	0.54	1.0	–	–	4.13	1.0	1.0
28	0.35	1.0	0.00	1.0	0.49	1.0	1.39	1.0	4.31	1.0	11.45	1.0	1.0
29	0.88	1.0	0.67	1.0	0.07	1.0	0.96	1.0	2.77	1.0	12.08	1.0	1.0
30	0.55	1.0	0.50	1.0	0.21	1.0	0.51	1.0	2.84	1.0	10.07	1.0	1.0
31	0.61	1.0	0.23	1.0	0.20	1.0	1.66	1.0	4.50	1.0	13.26	1.0	1.0
32	–	–	0.06	1.0	–	–	1.84	1.0	–	–	11.43	1.0	1.0
33	0.19	1.0	0.30	1.0	0.39	1.0	1.45	1.0	5.89	1.0	9.41	1.0	1.0
34	–	–	0.73	1.0	–	–	1.33	1.0	–	–	11.26	1.0	1.0
35	0.46	1.0	0.16	1.0	0.38	1.0	0.67	1.0	4.18	1.0	10.63	1.0	1.0
36	0.23	1.0	0.61	1.0	0.20	1.0	0.50	1.0	2.94	1.0	4.48	1.0	1.0
37	–	–	0.68	1.0	–	–	0.31	1.0	–	–	10.22	1.0	1.0
38	–	–	0.35	1.0	–	–	0.86	1.0	–	–	3.03	1.0	1.0
39	–	–	0.33	1.0	–	–	1.00	1.0	–	–	4.06	1.0	1.0
40	0.43	1.0	0.31	1.0	0.12	1.0	0.68	1.0	3.23	1.0	4.00	1.0	1.0
41	–	–	0.19	1.0	–	–	0.85	1.0	–	–	3.53	1.0	1.0
All	**0.51**	**1.0**	**0.43**	**1.0**	**0.26**	**1.0**	**0.84**	**1.0**	**3.62**	**1.0**	**7.74**	**1.0**	**1.0**

10. M.A. Zuluaga, I.E. Magnin, M. Hernández Hoyos, E.J.F. Delgado Leyton, F. Lozano, and M. Orkisz. Automatic detection of abnormal vascular cross-sections based on Density Level Detection and Support Vector Machines. *Int J Comput Assist Radiol Surg*, 6(2):163–174, 2011.